# Grupo de Inteligencia Computacional

Presentación en la Universidad Autónoma, Septiembre 2017

# Localization

The GIC belongs to the University of the Basque Country (UPV/EHU)
Located in Donostia-San Sebastian, Spain, Europe
Summary of group works: www.ehu.es/ccwintco > Historial de grupo

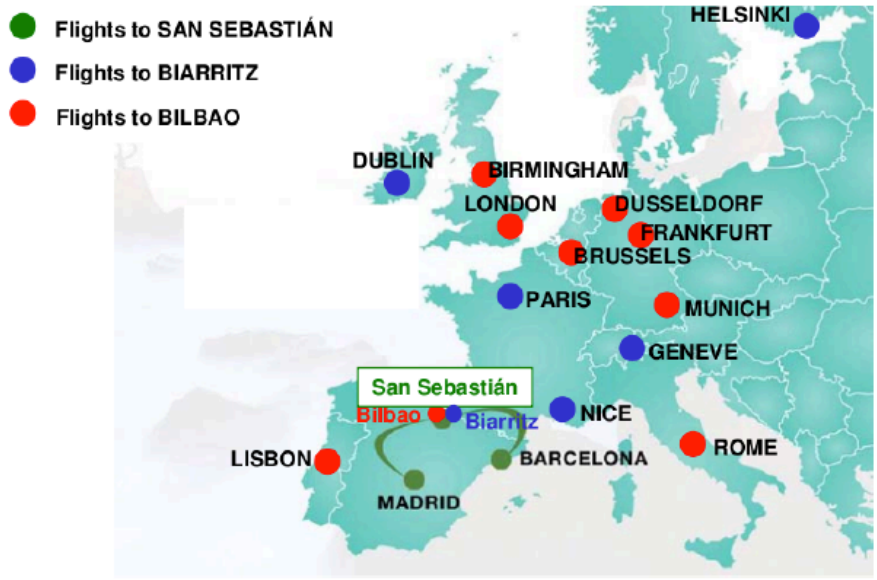

# Colaboradores

- Alex Savio: actualmente en la empresa privada desarrollando aplicaciones web
- Darya Chyzhyk: en el INRIA en Paris, trabajando sobre resting state fMRI y conectividad cerebral
- Maite Termenon: en la U Grenoble
- Maite Garcia: En CITA Alzheimer fundacion privada
- Leire Ozaeta: actualmente en Bulgaria en estancia preparando la tesis doctoral

# Contenido

- Recorrido por los resultados del GIC en los ultimos años
  - A Besga (H.U. Alava): Trastorno bipolar
  - AK Shin (Harvard U.): Esquizofrenia y alucinaciones
  - M Mataro, R Dacosta (U Barcelona): Stroke

# A Besga data

- Healthy, late onset BD, AD
- MRI image: T1, Difussion (FA), other (useless)
- Clinical and psychometric tests
- Blood biomarkers for inflammation and others

# General pipeline

- Using FSL
- Registration of T1 images
- Processing of DWI: registration, noise correction, computation of DTI, computation of DTI, extraction of FA
- Feature selection: anatomically located
- Classification to validate the predictive efficiency of localizations

Neurocomputing 114 (2013) 132–141

Contents lists available at SciVerse ScienceDirect

Neurocomputing

journal homepage: www.elsevier.com/locate/neucom

# Lattice independent component analysis feature selection on diffusion weighted imaging for Alzheimer's disease classification

M. Termenon [a], M. Graña [a,*], A. Besga [b,d], J. Echeveste [c,d], A. Gonzalez-Pinto [b,d]

[a] Grupo de Inteligencia Computacional, UPV/EHU, Spain
[b] Unidad de Investigación en Psiquiatría del Hospital de Santiago Apostol, Vitoria-Gasteiz, Spain
[c] Departamento de Resonancia Magnética, Osatek-Vitoria, Spain
[d] CIBERSAM, Spain

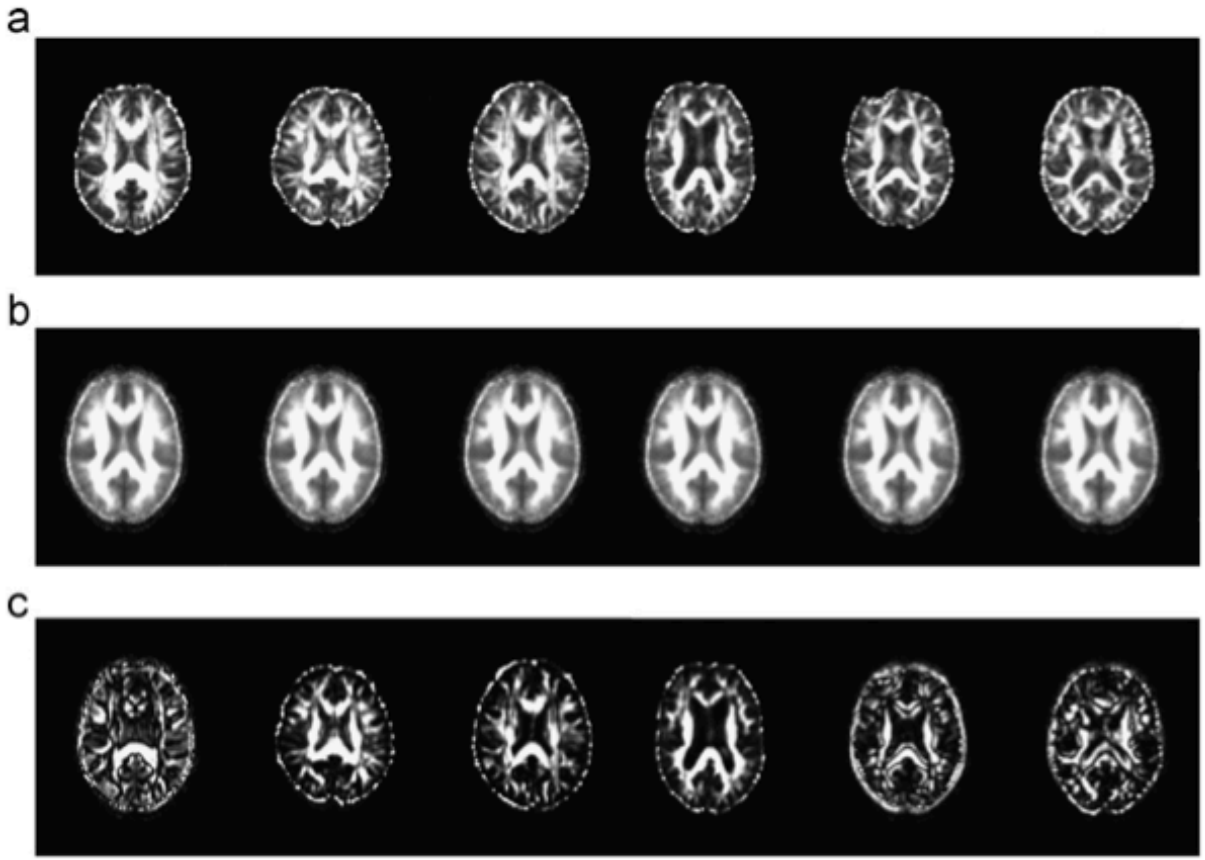




**Fig. 1.** Axial slices from three healthy controls and three AD patients. (a) Original FA volumes, (b) reconstructed volumes obtained computing the source mixing using the FLSU estimated abundance images $\hat{A}S$ and (c) residual error after the unmixing–mixing process obtained computing Eq. (3).

**Algorithm 1.** T1 and DWI data processing pipeline to obtain spatially normalized FA data.

1. Convert DICOM to nifti
2. Skull stripping T1-weighted volumes
3. Affine registration of T1-weighted skull stripped volumes to template MNI152.
4. Correct DWI scans.
5. Obtain skull stripped brain masks for each DWI corrected scans.
6. Apply diffusion tensor analysis computing DTI and FA.
7. Rigid registration 6DoF of FA data to T1-weighted normalized volumes, from Step3.

**Algorithm 2.** Computing the residual LICA.

1. Perform ILSIA on $I$ to induce the lattice independent sources $S$.
2. Compute FCLSU to obtain abundance matrix $\hat{A}$.
3. Compute the FA data reconstruction $\hat{I}$ from $S$ and $\hat{A}$: $\hat{I} = \hat{A}S$.
4. Obtain squared residual error between $I$ and $\hat{I}$: $R = (I - \hat{I})^2$.

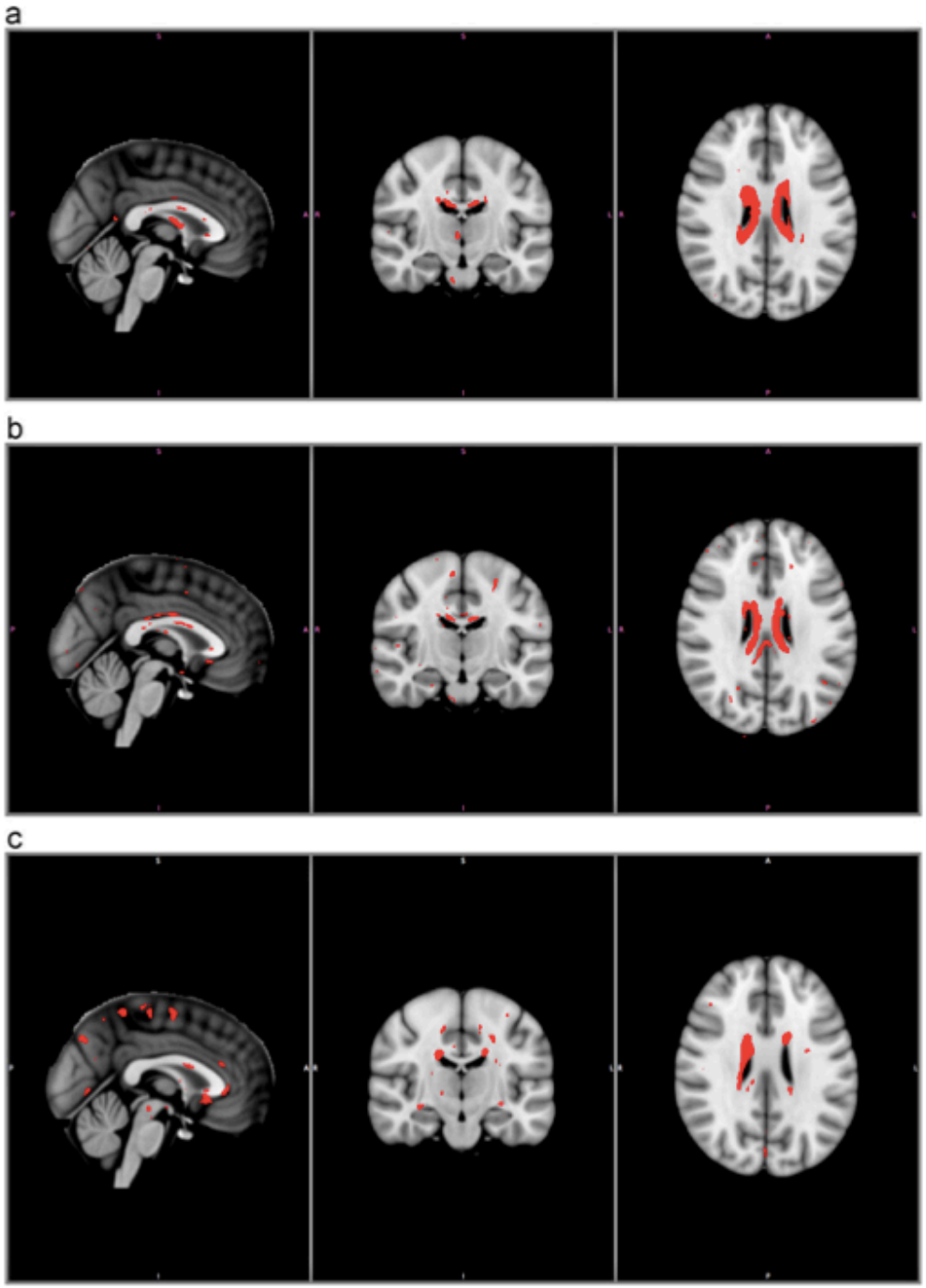


**Fig. 2.** Voxel sites for FA features selected with a 99.50% percentile on Pearson's correlation empirical distribution computed on (a) the original FA data, (b) the LICA residuals, (c) voxel based morphometry computed on the original FA data.

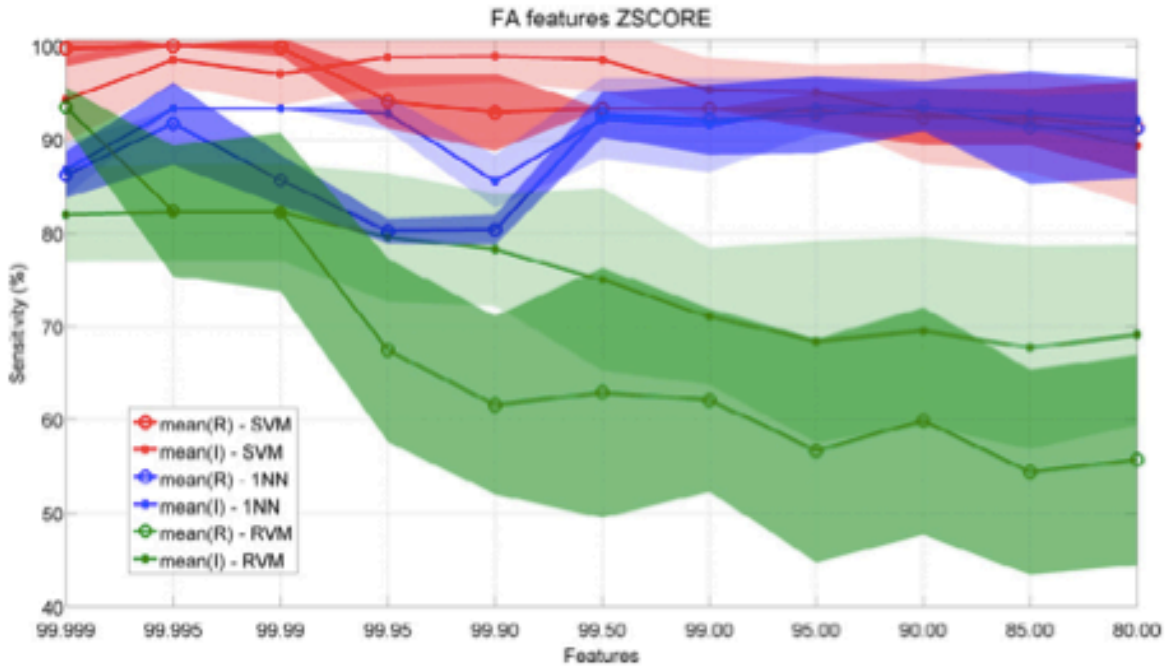


**Fig. 4.** Average classification sensitivity for features extracted from the FA data ($I$) and features extracted from the LICA residual ($R$) for varying percentiles on Pearson's correlation empirical distribution. In red, SVM classification results. In blue, 1NN classification results. In green, RVM classification results. (For interpretation of the references to color in this figure caption, the reader is referred to the web version of this article.)

frontiers in Aging Neuroscience

ORIGINAL RESEARCH
published: 16 June 2017
doi: 10.3389/fnag.2017.00179

# White Matter Tract Integrity in Alzheimer's Disease vs. Late Onset Bipolar Disorder and Its Correlation with Systemic Inflammation and Oxidative Stress Biomarkers

*Ariadna Besga[1,2]*, Darya Chyzhyk[3,4], Itxaso Gonzalez-Ortega[5,6], Jon Echeveste[7], Marina Graña-Lecuona[4], Manuel Graña[3,4] and Ana Gonzalez-Pinto[1,5,8]*

**Methods:** Fractional anisotropy (FA) coefficients are obtained from diffusion weighted imaging (DWI). Tract based spatial statistics (TBSS) finds FA skeleton clusters of WM tract voxels showing significant differences for all possible contrasts between HC, AD, and LOBD. An ANOVA *F*-test over all contrasts is carried out. Results of *F*-test are used to mask TBSS detected clusters for the AD > LOBD and LOBD > AD contrast to select the image clusters used for correlation analysis. Finally, Pearson's correlation coefficients between FA values at cluster sites and systemic blood plasma biomarker values are computed.

**Results:** The TBSS contrasts with by ANOVA *F*-test has identified strongly significant clusters in the forceps minor, inferior longitudinal fasciculus, inferior fronto-occipital fasciculus, and cingulum gyrus. The correlation analysis of these tract clusters found strong negative correlation of AD with the nerve growth factor (NGF) and brain derived neurotrophic factor (BDNF) blood biomarkers. Negative correlation of AD and positive correlation of LOBD with inflammation biomarker IL6 was also found.

**Conclusion:** TBSS voxel clusters tract atlas localizations are consistent with greater behavioral impairment and mood disorders in LOBD than in AD. Correlation analysis confirms that neurotrophic factors (i.e., NGF, BDNF) play a great role in AD while are absent in LOBD pathophysiology. Also, correlation results of IL1 and IL6 suggest stronger inflammatory effects in LOBD than in AD.

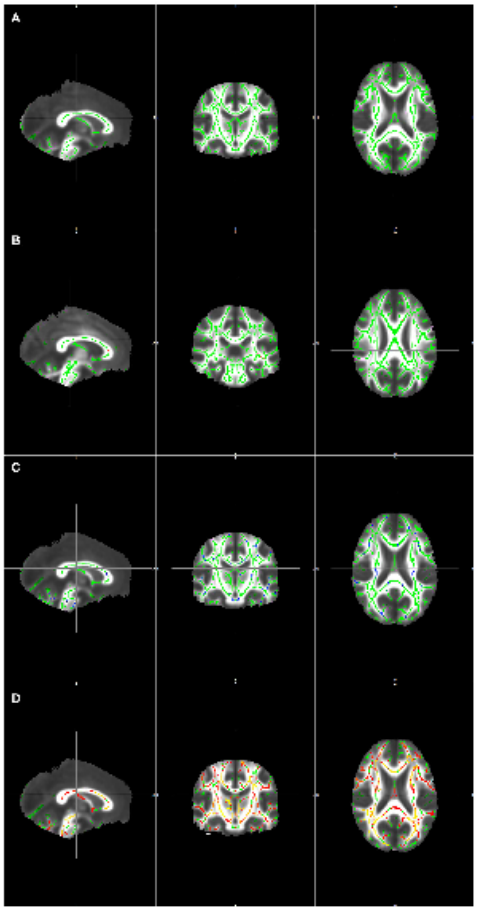


**RE 2 |** Visualization TBSS detection results masked by the *F*-test overlaid on the mean of registered FA volumes. **(A)** Mean skeleton (green). **(B)** F statistics slow) over the mean skeleton (green). **(C)** Clusters detected from contrast AD > LOBD masked by *F*-test clusters (blue) overlaying the mean skeleton (green). usters detected from contrast LOBD > AD masked by *F*-test clusters (red) overlaying the mean skeleton (green).

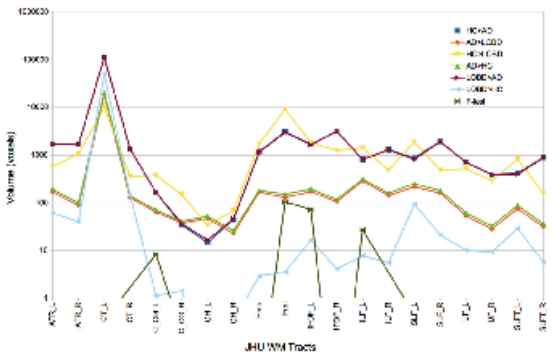


**FIGURE 1** | Size of FA skeleton clusters found by each contrast (HC > AD, AD > LOBD, HC > LOBD, AD > HC, LOBD > AD,LOBD > HC, *F*-test) of the permutation test followed by TFCE cluster inference for each tract identified by the JHU White-Matter Tractography Atlas. R, Right; L, left; ATR, hemispheres of anterior thalamic radiation; CT, corticospinal tract; C_CG, cingulum (cingulate gyrus); CH, Cingulum (hippocampus); FMI, forceps minor; FMa, forceps major; IFOF, inferior fronto-occipital fasciculus; ILF, inferior longitudinal fasciculus; SFL, superior longitudinal fasciculus; UF, uncinate fasciculus; SLFT, temporal part of SLF .

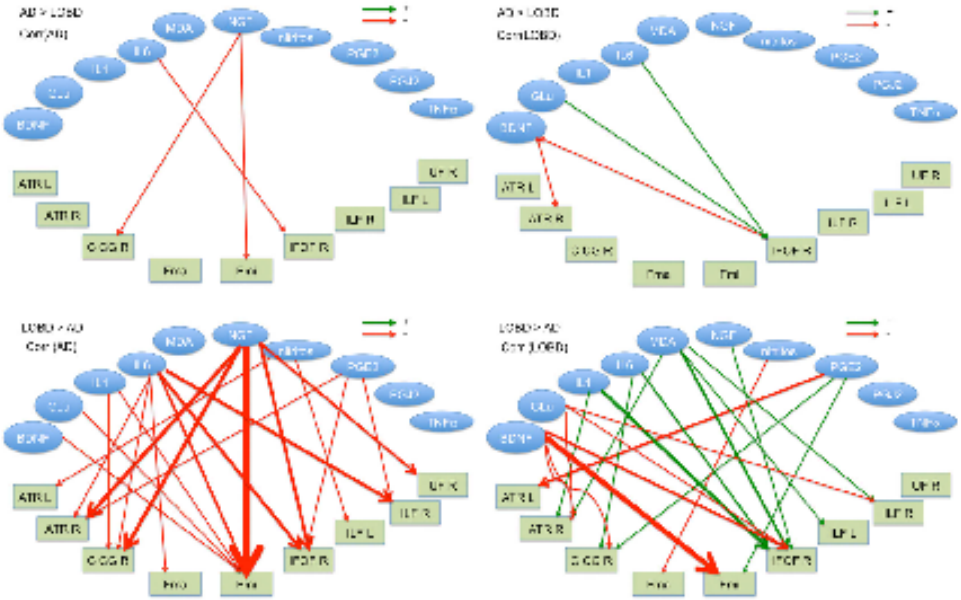

**FIGURE 3** | Significant correlation ($p < 0.01$) between blood plasma biomarkers (ellipses up) and FA values at the TBSS clusters for AD > LOBD (up) and LOBD > AD contrasts, masked by the *F*-test, identified by the atlasquery tool (rectangles below). We report separate values for AD and LOBD populations (requested by reviewer). Red lines correspond to negative correlations, green lines correspond to positive correlations. Line width is proportional to the magnitude of correlation. R, Right; L, left; ATR, hemispheres of anterior thalamic radiation; C_CG, cingulum (cingulate gyrus); FMI, forceps minor; FMa, forceps major; IFOF, inferior fronto-occipital fasciculus; ILF, inferior longitudinal fasciculus; SFL, superior longitudinal fasciculus; and UF, uncinate fasciculus.

FINAL

*Send Orders for Reprints to reprints@benthamscience.ae*

*Current Alzheimer Research*, 2016, *13*, 000-000



# Eigenanatomy on Fractional Anisotropy Imaging Provides White Matter Anatomical Features Discriminating Between Alzheimer's Disease and Late Onset Bipolar Disorder

Ariadna Besga[1,2,3,*], Darya Chyzhyk[5,8], Itxaso González-Ortega[1,2,4], Alexandre Savio[5,7], Borja Ayerdi[5,9], Jon Echeveste[6], Manuel Graña[5,7] and Ana González-Pinto[1,2,3]

[1]*Department of Psychiatry, University Hospital of Alava-Santiago, Vitoria, Spain;* [2]*Centre for Biomedical Research Network on Mental Health (CIBERSAM), Spain;* [3]*School of Medicine, University of the Basque Country, Vitoria, Spain;* [4]*School of Psychology, University of the Basque Country, San Sebastián, Spain;* [5]*Computational Intelligence Group (GIC), University of the Basque Country (UPV/EHU), San Sebastián, Spain;* [6]*Magnetic Resonance Imaging Department, Osatek-Vitoria;* [7]*ENGINE project, Wroclaw Technological University, Poland;* [8]*CISE Department, Unuversity of Florida, Gainesville, USA;* [9]*ACPySS, San Sebastian, Spain*

Ariadna Besga

**Abstract:** ***Background:*** Late Onset Bipolar Disorder (LOBD) is the arousal of Bipolar Disorder (BD) at old age (>60) without any previous history of disorders. LOBD is often difficult to distinguish from

Eigenanatomy feature extraction

- partial sparse canonical correlation analysis (PSCCAN)
- provided in the ANTS open source neuroimage suite
- SCCAN looks for the projection maximizing the correlation between two datasets of paired observations

SCCAN looks for the projection directions $\psi_X$ and $\psi_Y$ maximizing the Pearson's correlation after the whitening transform of the datasets, i.e.

$$x^*, y^* = \arg\max_{\psi_X, \psi_Y} \frac{\psi_X^T \Sigma_{X_w Y_w} \psi_Y}{\|\psi_X\| \|\psi_y\|}, \quad (1)$$

subject to sparseness constraints on the image eigenvectors $\|\psi_X\|_1 < s$, where $\|.\|_1$ denotes the $\|.\|_1$ norm, and s is the sparseness level, $\Sigma_{X_w Y_w} = X_w^T Y_w$ is the correlation matrix of the datasets after whitening, i.e. $X_w = X\Sigma_{XX}^{1/2}$ and $Y_w = Y\Sigma_{YY}^{1/2}$. PSCCAN considers also the confound variables in matrix Z of dimensions $n \times q^1$, seeking the optimal correlation after removing the effect of the confounding variables, i.e.

$$x^*, y^* = \arg\max_{\psi_X, \psi_Y} \frac{\psi_X^T \Sigma^{\setminus Z}_{X_w Y_w} \psi_Y}{\|\psi_X\| \|\psi_Y\|}, \quad (2)$$

where $\Sigma^{\setminus Z}_{X_w Y_w}$ is the variance-covariance matrix of the whitened residuals of the data after removing the confounding variables, $X_w = X\left(\Sigma^{\setminus Z}_{XX}\right)^{-1/2}$ and $Y_w = Y\left(\Sigma^{\setminus Z}_{YY}\right)^{-1/2}$. The residual covariance is computed as $\Sigma^{\setminus Z}_{X_w Y_w} = X^T Y - X^T Z_w Z_w^T Y$. Opti-

In our study, the Y matrix is composed of the values corresponding to one biomarker, hence we perform independent localizations for each; the confounding variables in Z are age and gender.

**Table 2.** **Classification cross-validation average results for the PSCCAN coefficients maximally correlated to each plasma biomarker. Columns: L Linear SVM, RBF best SVM-RBF result obtained after model search for the RBF width, enclosed in brackets.**

| | | Accuracy | | F score | | Sensitivity | | Specificity | |
|---|---|---|---|---|---|---|---|---|---|
| | | L | RBF | L | RBF | L | RBF | L | RBF |
| MDA | HC vs. AD | 76.6 | 81.4 | 65.0 | 72.4 | 65.0 | 71.7 | 83.3 | 84.4 |
| | AD vs. LOBD | 78.3 | 85.3 | 80.9 | 86.7 | 80.8 | 87.3 | 81.6 | 87.4 |
| | HC vs. D+LOBD | 67.1 | 76.3 | 52.2 | 57.7 | 65.0 | 70.7 | 69.3 | 73.0 |
| | HC vs. LOBD | 58.0 | 66.8 | 33.3 | 40.1 | 35.0 | 39.6 | 81.6 | 85.4 |
| BDNF | HC vs. AD | 68.6 | 74.7 | 59.0 | 61.7 | 70.0 | 75.2 | 72.5 | 77.4 |
| | AD vs. LOBD | 69.6 | 76.7 | 72.1 | 77.9 | 70.0 | 74.2 | 78.3 | 84.1 |
| | HC vs. DAD+LOBD | 60.5 | 70.1 | 46.2 | 51.5 | 70.0 | 75.8 | 63.3 | 67.5 |
| | HC vs. LOBD | 49.5 | 60.4 | 54.6 | 58.2 | 70.0 | 73.8 | 43.3 | 58.6 |
| NOx | HC vs. AD | 65.7 | 72.3 | 55.2 | 59.7 | 65.0 | 68.9 | 71.6 | 76.3 |
| | AD vs. LOBD | 66.3 | 73.3 | 66.9 | 72.2 | 63.3 | 67.4 | 80.0 | 86.1 |
| | HC vs. AD+LOBD | 65.8 | 71.3 | 49.7 | 58.2 | 60.0 | 62.0 | 71.6 | 75.5 |
| | HC vs. LOBD | 56.0 | 65.6 | 52.0 | 59.7 | 65.0 | 71.4 | 56.6 | 61.6 |
| Glu | HC vs. AD | 69.0 | 76.7 | 58.0 | 61.6 | 70.0 | 75.3 | 75.8 | 81.3 |
| | AD vs. LOBD | 74.6 | 81.1 | 77.3 | 85.3 | 79.2 | 83.4 | 75.0 | 81.1 |
| | HC vs. AD+LOBD | 69.1 | 78.7 | 45.3 | 51.0 | 55.0 | 61.3 | 76.6 | 83.1 |
| | HC vs. LOBD | 58.5 | 67.1 | 40.3 | 45.2 | 50.0 | 53.2 | 76.6 | 81.6 |
| IL1β | HC vs. AD | 66.6 | 72.9 | 55.6 | 61.3 | 65.0 | 69.8 | 72.5 | 76.0 |
| | AD vs. LOBD | 71.3 | 79.1 | 73.7 | 78.4 | 71.7 | 76.4 | 76.6 | 80.8 |
| | HC vs. AD+LOBD | 64.3 | 70.4 | 45.5 | 50.3 | 65.0 | 70.3 | 66.6 | 70.5 |
| | HC vs. LOBD | 54.5 | 63.2 | 48.0 | 54.4 | 65.0 | 70.3 | 63.3 | 70.6 |
| IL6 | HC vs. AD | 75.3 | 80.7 | 66.6 | 73.0 | 70.0 | 74.1 | 83.3 | 87.6 |
| | AD vs. LOBD | 71.6 | 78.2 | 71.9 | 78.3 | 68.3 | 73.2 | 81.6 | 87.3 |
| | HC vs. AD+LOBD | 69.3 | 76.4 | 47.0 | 52.6 | 65.0 | 69.8 | 73.0 | 77.8 |
| | HC vs. LOBD | 60.5 | 68.9 | 51.6 | 55.3 | 50.0 | 55.6 | 81.6 | 87.4 |
| TNFα | HC vs. AD | 71.3 | 78.3 | 69.4 | 75.1 | 80.0 | 86.0 | 70.8 | 75.0 |
| | AD vs. LOBD | 66.0 | 72.5 | 66.7 | 73.3 | 64.2 | 70.3 | 78.3 | 81.8 |
| | HC vs. AD+LOBD | 63.4 | 70.0 | 45.3 | 50.7 | 65.0 | 69.1 | 66.6 | 70.1 |
| | HC vs. LOBD | 49.5 | 55.3 | 54.7 | 60.7 | 75.0 | 80.0 | 56.6 | 62.0 |

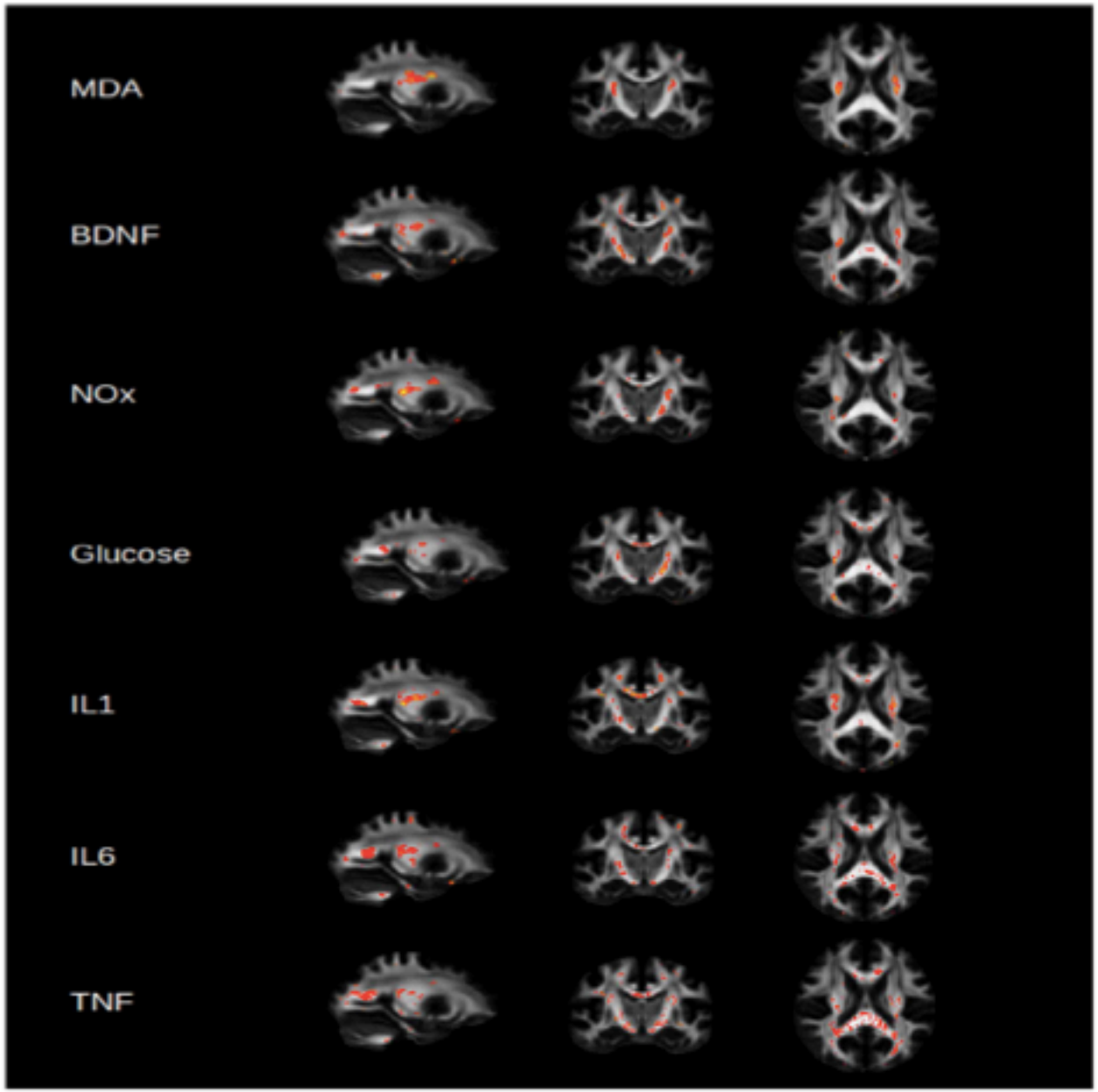


**Fig. (1).** Localization of the first eigenvectors maximally correlated with the corresponding biomarker visualized over the Fractional Anisotropy template, from left to right sagittal, coronal, and axial views.

frontiers in Aging Neuroscience

ORIGINAL RESEARCH
published: 14 December 2015
doi: 10.3389/fnagi.2015.00231

# Discrimination between Alzheimer's Disease and Late Onset Bipolar Disorder Using Multivariate Analysis

*Ariadna Besga[1,2,3]*, Itxaso Gonzalez[1,2,4], Enrique Echeburua[2,4], Alexandre Savio[5,6], Borja Ayerdi[5], Darya Chyzhyk[5,7], Jose L. M. Madrigal[2,8], Juan C. Leza[2,8], Manuel Graña[5,6,9] and Ana Maria Gonzalez-Pinto[1,2]*

**TABLE 2 | Welch's *t*-test *p*-value for each behavioral, biological biomarker, and aggregate neuropsychological variable (rows) *per* group contrast (columns).**

| | HC vs. AD | HC vs. LOBD | LOBD vs. AD |
|---|---|---|---|
| **CLINICAL** | | | |
| FAST | <0.001 | <0.001 | <0.001 |
| TD1 | 0.022 | 0.045 | 0.871 |
| TA1 | 0.009 | <0.001 | 0.002 |
| TDD | 0.002 | <0.001 | 0.145 |
| TA2 | 0.002 | <0.001 | 0.110 |
| TE | 0.325 | 0.008 | 0.026 |
| TA3 | <0.001 | <0.001 | 0.579 |
| TD2 | 0.065 | 0.356 | 0.618 |
| TI | 0.003 | 0.001 | 0.068 |
| TC | 0.003 | 0.096 | 0.230 |
| TS | 0.001 | 0.004 | 0.088 |
| **BIOLOGICAL BIOMARKER** | | | |
| BDNF | 0.631 | 0.263 | 0.425 |
| NGF | 0.090 | 0.916 | 0.074 |
| $NO_2$ | 0.468 | 0.233 | 0.763 |
| TNFα | 0.087 | 0.691 | 0.021 |
| IL6 | 0.646 | 0.147 | 0.170 |
| IL1 | 0.539 | 0.781 | 0.477 |
| MDA | 0.304 | 0.052 | <0.001 |
| **NEUROPSY** | | | |
| EF | <0.001 | <0.001 | 0.337 |
| A | <0.001 | <0.001 | 0.804 |
| M | <0.001 | <0.001 | <0.001 |

*Statistically significant entries ($p < 0.01$) are highlighted in gray.*
*TD1, total delusions; TA1, total agitation; TDD, total dysphoria/depression; TA2, total anxiety; TE, total euphoria; TA3, total apathy; TD2, total disinhibition; TI, total irritability; TC, total CMA; TS, total sleep; EF, executive functions; A, attention; M, memory.*

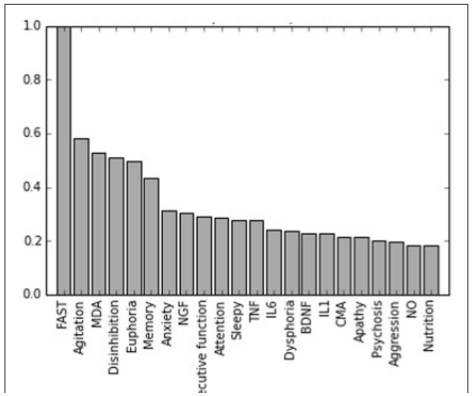


**TABLE 3 | LOO accuracy estimation of the classifiers on the various combinations of features for each classification contrast.**

| | | CART | RF | SVM (rbf) | SVM (lin) |
|---|---|---|---|---|---|
| LOBD vs. AD | 1. BIO | 46.38 | 59.42 | 71.01 | 60.87 |
| | 2. NEURO | 66.67 | 71.01 | 68.12 | 55.07 |
| | 3. BEHAV | 85.51 | 84.06 | 79.71 | 84.06 |
| | 4. BIO + NEURO | 66.67 | 62.32 | 71.01 | 66.67 |
| | 5. BIO + BEHAV | 79.71 | 73.91 | 79.71 | 79.71 |
| | 6. NEURO + BEHAV | 79.71 | 81.16 | 82.61 | 84.06 |
| | 7. NEURO + BEHAV + BIO | 78.26 | 79.71 | 84.06 | 82.61 |
| | 8. NEURO + BEHAV + BIO-Wt | **90.26** | **86.67** | **89.06** | **87.51** |
| HC vs. AD | 1. BIO | 71.43 | 60.32 | 57.14 | 49.21 |
| | 2. NEURO | 88.89 | 93.65 | 87.30 | 84.13 |
| | 3. BEHAV | 95.24 | 95.24 | 93.65 | 95.24 |
| | 4. BIO + NEURO | 85.71 | 87.30 | 87.30 | 88.89 |
| | 5. BIO + BEHAV | 92.06 | 92.06 | 96.83 | 93.65 |
| | 6. NEURO + BEHAV | 93.65 | 96.83 | 95.24 | 96.83 |
| | 7. NEURO + BEHAV + BIO | 95.24 | 95.24 | 95.24 | 92.06 |
| | 8. NEURO + BEHAV + BIO-Wt | **96.24** | **97.21** | **97.21** | **97.21** |
| HC vs. LOBD | 1. BIO | 46.55 | 48.28 | 53.45 | 60.34 |
| | 2. NEURO | 75.86 | 77.59 | 79.31 | 82.76 |
| | 3. BEHAV | 89.66 | 89.66 | 91.38 | 91.38 |
| | 4. BIO + NEURO | 79.31 | 82.76 | 77.59 | 77.59 |
| | 5. BIO + BEHAV | 82.76 | 93.10 | 91.38 | 91.38 |
| | 6. NEURO + BEHAV | 82.76 | 94.83 | 93.10 | 93.10 |
| | 7. NEURO + BEHAV + BIO | 82.76 | 89.66 | 93.10 | 91.38 |
| | 8. NEURO + BEHAV + BIO-Wt | **91.76** | **95.76** | **94.10** | **94.38** |

*Bold values are the maximum attained by a classifier per classification contrast.*
*BIO, blood biomarkers; BEHAV, clinical variables; NEURO, neuropsychological tests; Wt variables are selected according to Welch's t-test.*

# AK Shinn

- Data about people with schizophrenia with and without hallucination
- Resting state fMRI
- Connectivity results
- Dynamic causal analysis

International Journal of Neural Systems, Vol. 25, No. 3 (2015) 1550007 (23 pages)

DOI: 10.1142/S0129065715500070

World Scientific
www.worldscientific.com

**Discrimination of Schizophrenia Auditory Hallucinators by Machine Learning of Resting-State Functional MRI**

Darya Chyzhyk* and Manuel Graña
*Computational Intelligence Group*
*Universidad del Pais Vasco (UPV/EHU)*
*San Sebastian 20018, Spain*
**darya.chyzhyk@ehu.es*

Döst Öngür and Ann K. Shinn
*McLean Hospital, Belmont, MA, USA*
*Harvard Medical School, Boston, MA, USA*

Accepted 14 January 2015
Published Online 10 March 2015

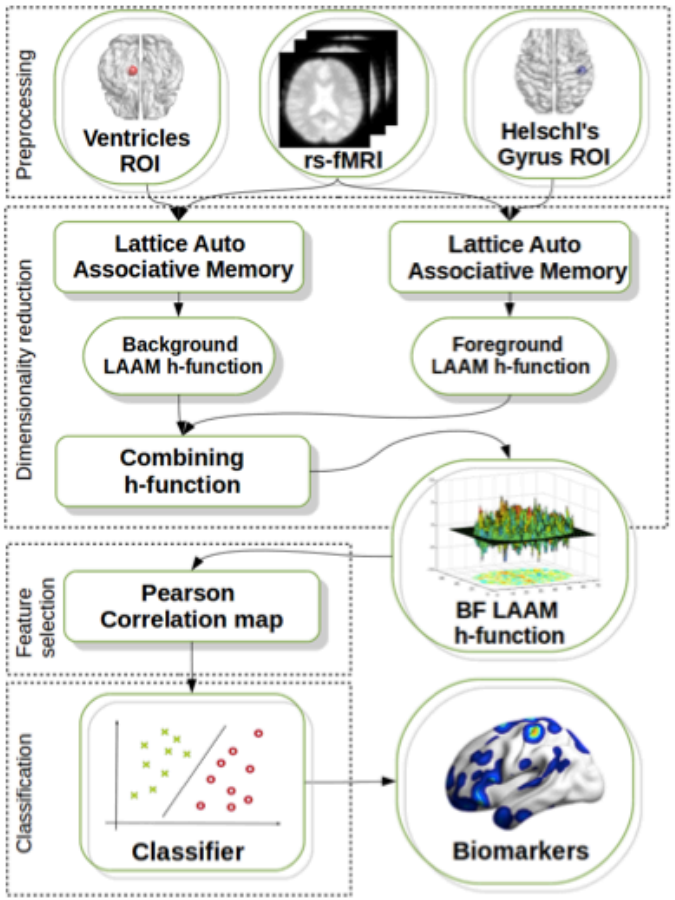


Fig. 1. Analysis pipeline for the background/foreground (BF)-LAAM-based FC approach. (1) rsfMRI data were preprocessed, and time series extracted from the specific background (cerebrospinal fluid, CSF) and foreground (right or left Heschl's gyrus) regions of interest (RoIs). (2) We then performed dimensionality reduction, reducing the high dimensionality time series data into LAAM-based FC measures. (3) We performed feature selection and extraction, using the Pearson's correlation coefficient ($r$) between the voxel value across subjects and the class label as a saliency measure to select the voxel sites with the greatest discriminative power. (4) We performed classification using support vector machines (SVM), and generate spatial maps showing the voxel sites with the features that are most highly discriminative.

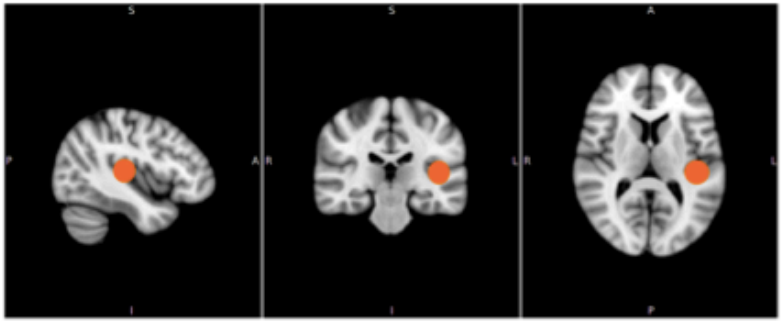

(a)

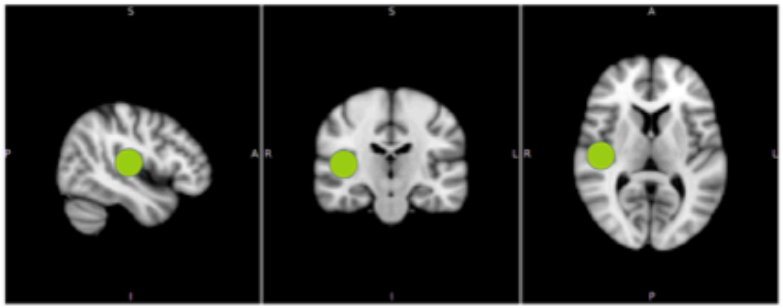

(b)

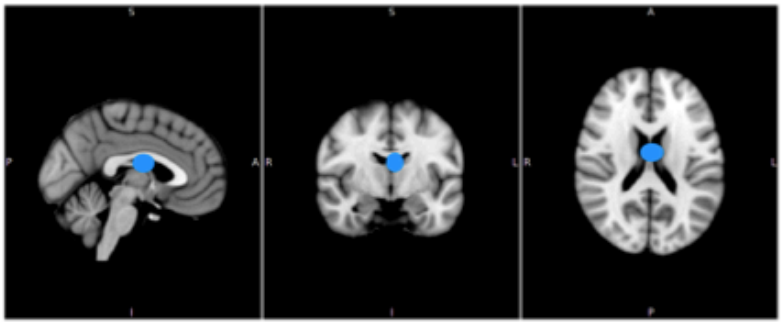

(c)

Fig. 2. The ROIs used for LAAM based connectivity analysis. The fMRI time series from LHG (10 mm, MNI coordinates $[-42, -26, 10]$) (a) and RHG (10 mm, MNI coordinates $[46, -20, 8]$) (b) were used to compute the left and right OS-LAAM $h$-functions, respectively. We also computed the BF-LAAM $h$-functions, where the fMRI time series from the CSF (10 mm, MNI coordinates $[-15, -26, 10]$) (c) was set as the background training dataset and the fMRI time series from the LHG (a) or RHG (b) were set as the foreground training dataset.

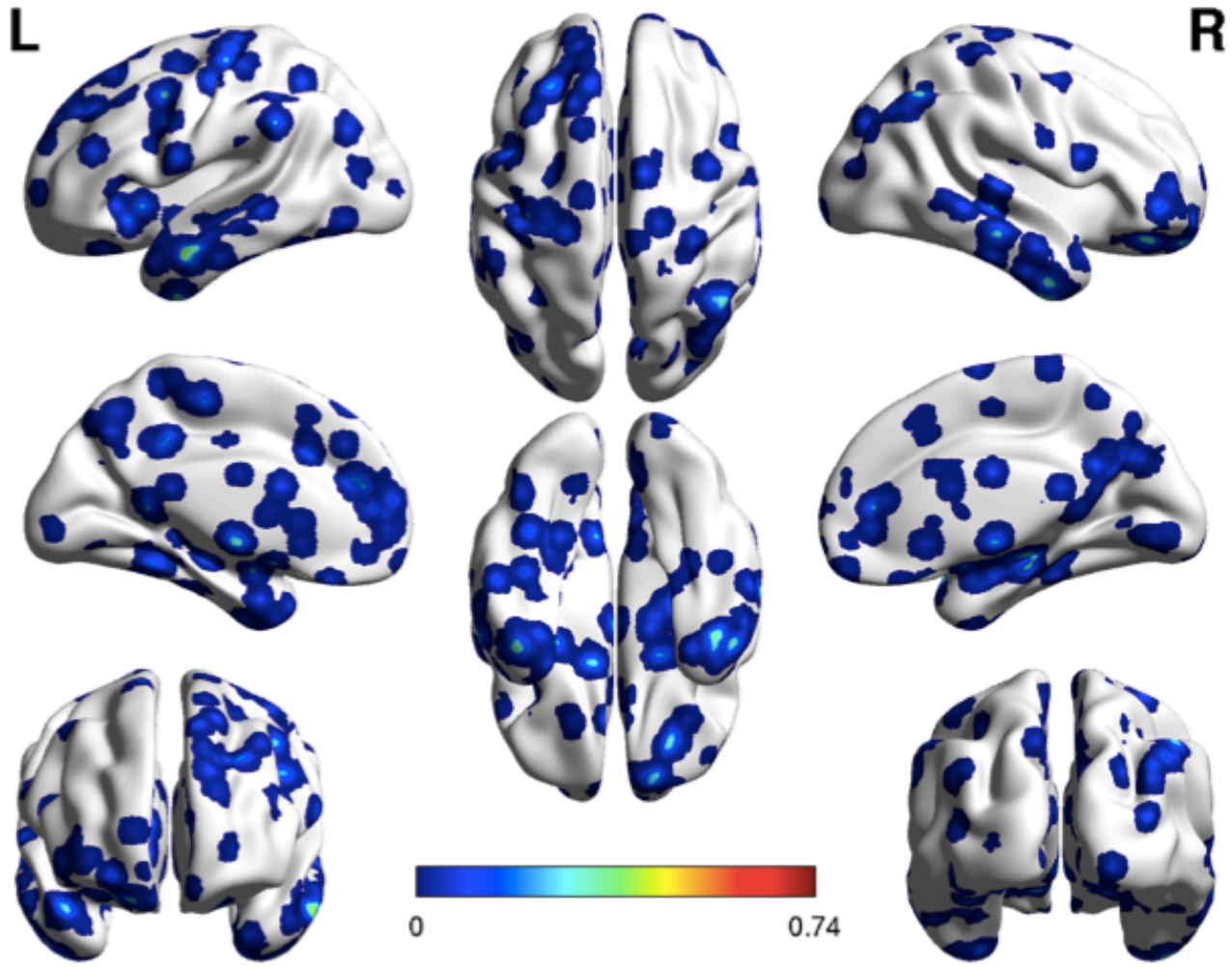


Fig. 3. (Color online) Localization of feature voxel sites selected from the BF-LAAM $h$-function map with foreground seed extracted from the LHG ROI, when discriminating SZAH from SZnAH populations. Colorbar is proportional to voxel saliency.

Table 1. Average accuracy of cross-validation results, feature vector size *per* columns.

| | Measure | Feat. Map. | HG | 500 | 1000 | 5000 | 10,000 |
|---|---|---|---|---|---|---|---|
| SZAH versus SZNAH | FC | OS-LAAM | L | **97.5** | **97.5** | **97.5** | **92.5** |
| | | | R | **92.5** | **92.5** | **95** | **95.2** |
| | | BF-LAAM | L | **100** | **97.5** | **95** | **90** |
| | | | R | **100** | **100** | **100** | **100** |
| | LA | ReHo | — | **100** | **100** | **100** | **100** |
| | | ALFF | — | 85 | 87.5 | **92.5** | **92.5** |
| | | fALFF | — | **97.5** | **100** | **100** | **97.5** |
| SZAH versus HC | FC | OS-LAAM | L | 43.7 | 42.7 | 30.7 | 28.3 |
| | | | R | 52.3 | 50 | 33 | 28 |
| | | BF-LAAM | L | **96.7** | **98** | **96.3** | **93** |
| | | | R | **98.3** | **96** | **92.7** | **93** |
| | LA | ReHo | — | **98** | **98.3** | **96.7** | **96.6** |
| | | ALFF | — | 48.7 | 49 | 30.3 | 31.7 |
| | | fALFF | — | **100** | **100** | **98.3** | **98.3** |
| SZNAH versus HC | FC | OS-LAAM | L | 65 | 63 | 59.5 | 55 |
| | | | R | 74 | 70 | 60 | 55 |
| | | BF-LAAM | L | **100** | **100** | **95.5** | **93** |
| | | | R | **100** | **98** | **95.5** | **93.5** |
| | LA | ReHo | — | **97.5** | **98** | **95.5** | **96** |
| | | ALFF | — | 78 | 76 | 62 | 53 |
| | | fALFF | — | **100** | **100** | **100** | **100** |
| SZ versus HC | FC | OS-LAAM | L | 32.4 | 31 | 26 | 25 |
| | | | R | 41.4 | 36.7 | 26.9 | 25.2 |
| | | BF-LAAM | L | **95.5** | **97.1** | 88.6 | 85.7 |
| | | | R | **94.3** | **91.2** | 86.7 | 87.1 |
| | LA | ReHo | — | **95.7** | **95.7** | **97** | **95.5** |
| | | ALFF | — | 48.8 | 42.9 | 35.2 | 35.2 |
| | | fALFF | — | **98.5** | **100** | **97.1** | **97.1** |

*Note*: Rows correspond to scalar feature mappings. Column HG indicates the left (L) or right (R) Heschl's Gyrus ROI. Results above 90% are highlighted in bold. Key to abbreviations: FC = Functional connectivity, LA = Local Activity, OS-LAAM = one-sided lattice auto-associative memories, BF-LAAM = background/foreground lattice auto-associative memories, ReHo = regional homogeneity, ALFF = amplitude of low frequency fluctuations, fALFF = fractional amplitude of low frequency fluctuations.

International Journal of Neural Systems, Vol. 27, No. 1 (2017) 1750019 (15 pages)

DOI: 10.1142/S0129065717500198

World Scientific
www.worldscientific.com

# Resting State Effective Connectivity Allows Auditory Hallucination Discrimination

Manuel Graña*,‡,§, Leire Ozaeta* and Darya Chyzhyk*,†,‡
*Computational Intelligence Group
University of the Basque Country, UPV/EHU, Spain
†CISE Department, University of Florida, Gainesville, USA
‡ACPySS, San Sebastian, Spain
§manuel.grana@ehu.es

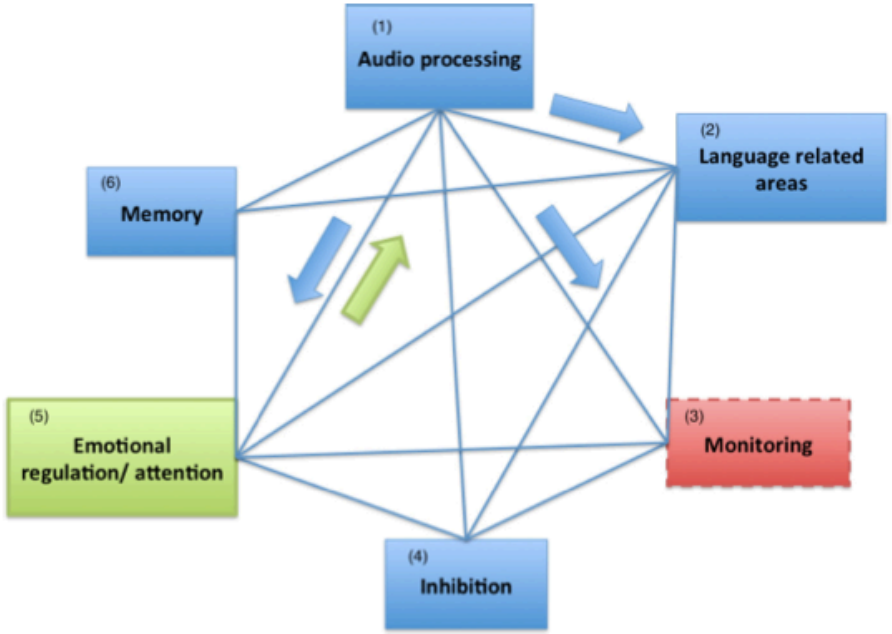


Fig. 1. Abstract functional model of the brain functional interactions while experiencing an AH. The arrows indicate the general expected hallucinating signal path, starting in the auditory cortex and traveling to emotional regulation/attention, language related and monitoring areas. The areas with thicker border are more activated in the hallucination prone brain, while areas with dotted border are less activated.

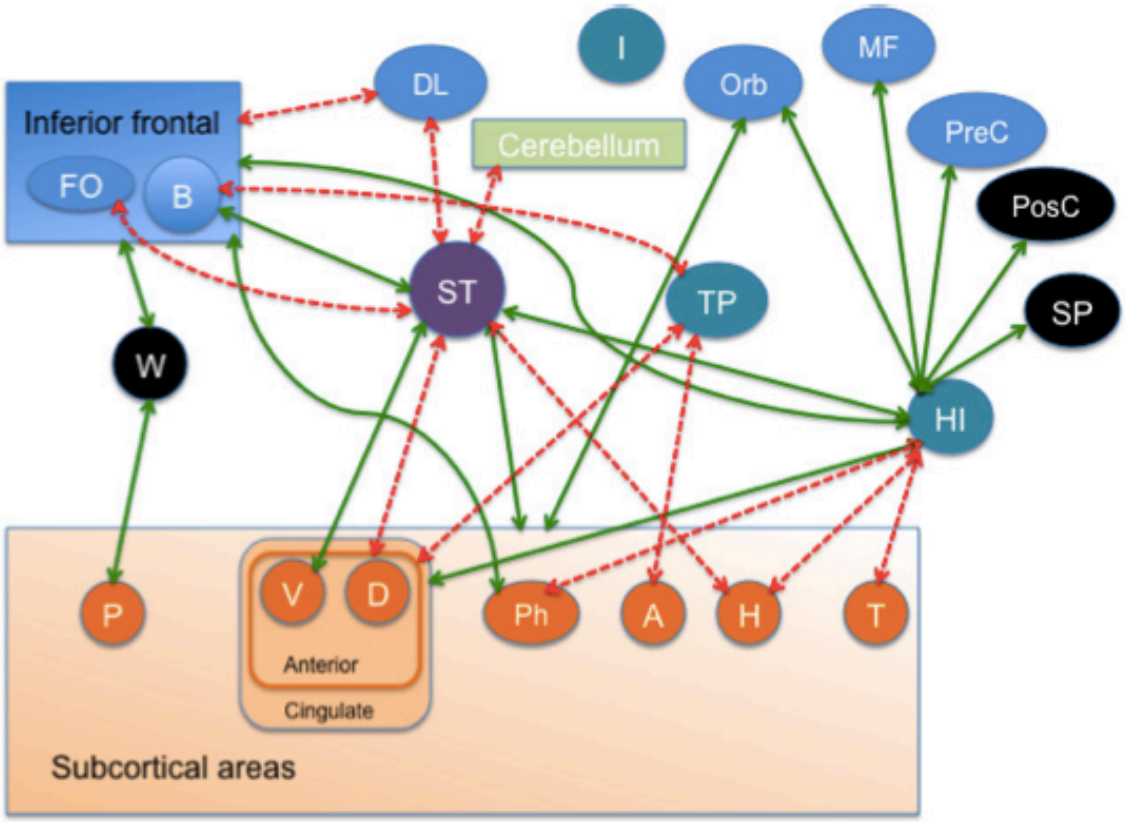


Fig. 2. (Color online) A detailed anatomical network of interacting brain regions underlying the abstract functional generative mechanism of auditive hallucinations. Identified areas are as follows: orbitofrontal gyrus (Obr), frontal dorsolateral gyrus (DL), middle frontal gyrus (MF), precentral gyrus (PreC), Broca's area (B), frontal operculum (FO), superior parietal (SP), Wernickle's area (W), postcentral gyrus (PostC), amygdala (A), Thalamus (T), putamen (P), ventral anterior cingulate (V), dorsal anterior cingulate (D), hippocampus (H), parahippocamus (Ph), insula (I), Heschl's gyrus (Hl), Temporoparietal gyrus (TP), superior temporal (ST). Continuous green line connections are stronger in the hallucinating brain. Dotted red line connections are weaker in the hallucinating brain.

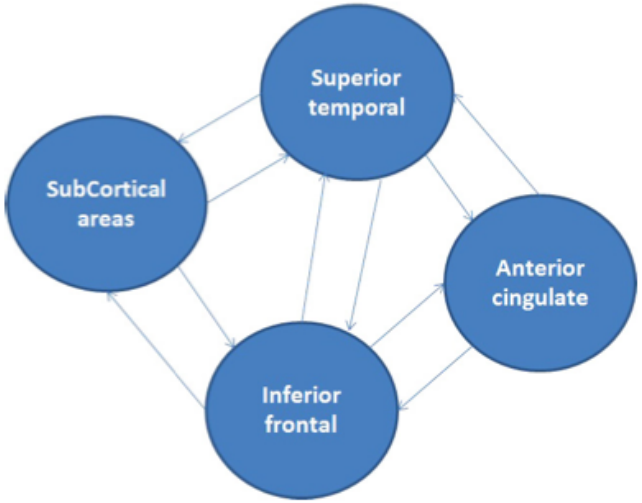


Fig. 3. The simplified anatomical model of interacting brain regions used for DCM estimation of effective connectivity parameters.

*Dynamic causal modeling*

$$\dot{\mathbf{x}} = \mathbf{A}\mathbf{x} + \sum_{j=1}^{m} \mathbf{u}_j \mathbf{B}_j \mathbf{x} + \mathbf{C}\mathbf{u},$$

$$\dot{\mathbf{x}} = \mathbf{A}\mathbf{x} + \mathbf{B}\mathbf{v},$$

### 3.2. *Granger causality*

$$\mathbf{x}(t) = \sum_{i=1}^{p} \mathbf{A}(i)\mathbf{x}(t-i) + \mathbf{E}(t),$$

$$\mathrm{PDC}_{ij}(\omega) = \frac{\bar{\mathbf{A}}_{ij}(\omega)}{\sqrt{\bar{\mathbf{a}}_j^{H}(\omega)\bar{\mathbf{a}}_i(\omega)}},$$

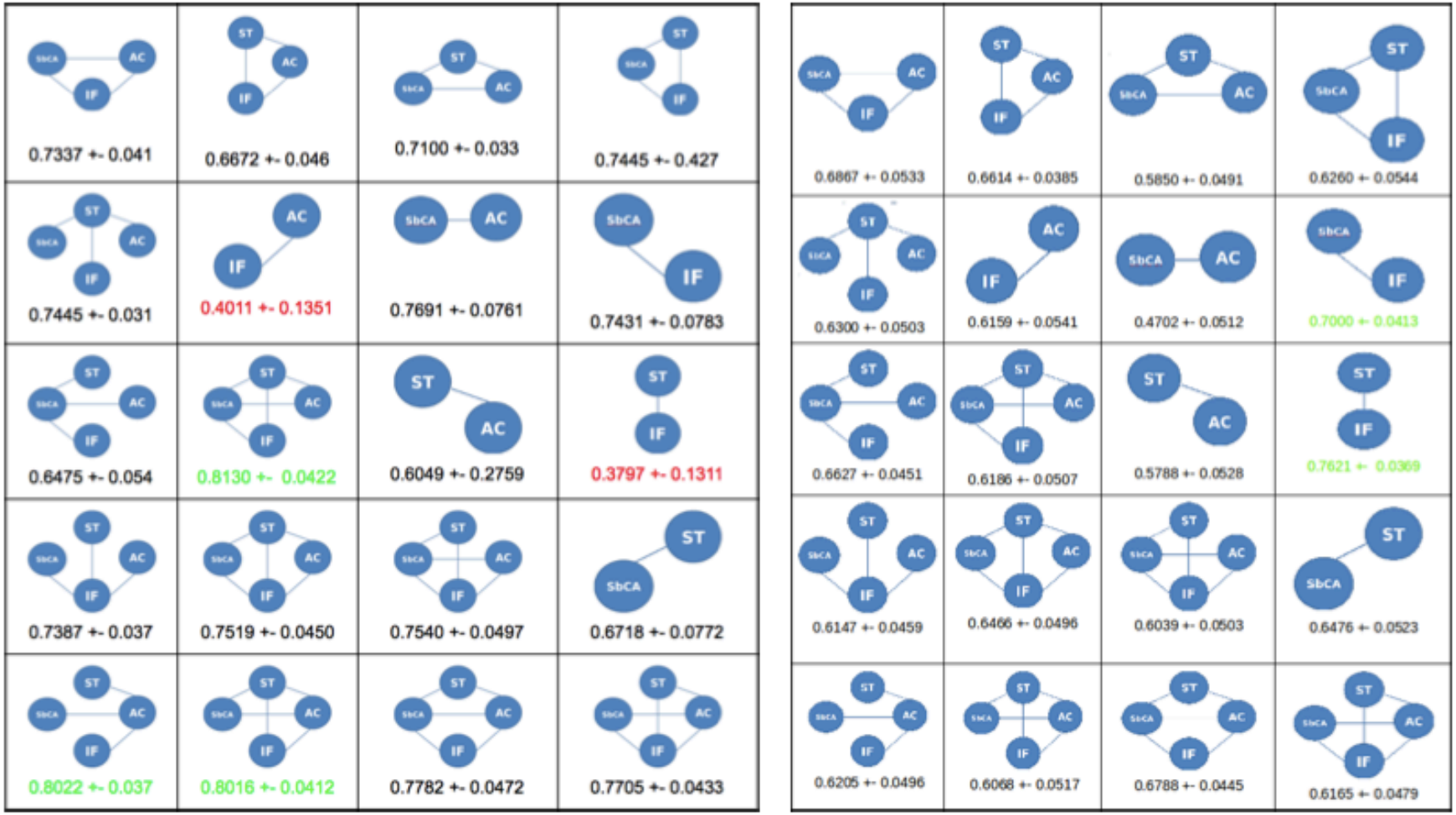


(a) (b)

Fig. 4. (Color online) Results of the connection selection, testing all possible networks of effective connections. Below each network graphical representation, we give the average and standard deviation of accuracy results of cross-validation of a linear SVM classifier over their respective feature vectors. Average accuracy values above 80% and 70% for DCM-CCF and GC-PDC features, respectively, are highlighted in green. (a) Results using DCM-CCF features, (b) results using GC-PDC features. The features for each connection are the complete set of coefficients. Red values highlight results that are worst than a pure random classifier.

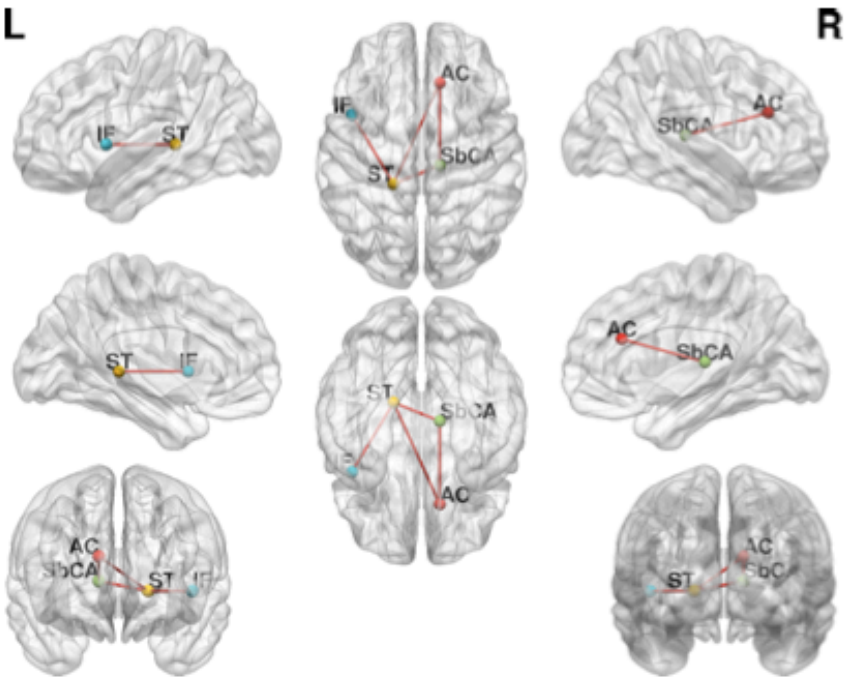


Fig. 5. (Color online) Visualization of the brain localization of the effective connection network achieving the highest accuracy discriminating hallucination prone brains considering all the DCM-CCF coefficients per connection.

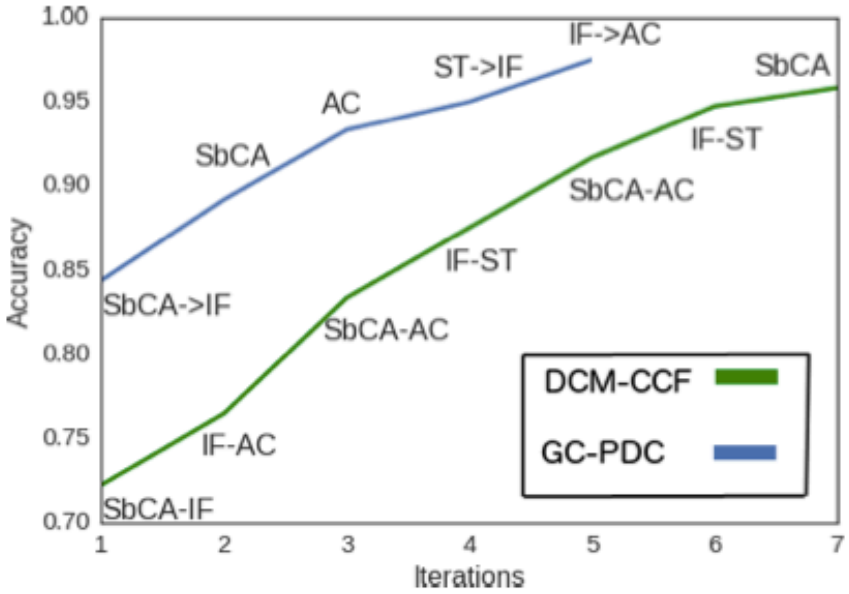


Fig. 6. (Color online) LOO cross-validation estimated accuracy at each iteration of the greedy wrapper feature selection process applied to each frequency independently. Labels shown on the plot correspond to the connection added at this iteration. The blue plot corresponds to the results achieved with GC-PDC features, the green plot to the results of using DCM-CCF features.

# GRACIAS POR SU ATENCION